TRABAJO DE FIN DE GRADO

GRADO EN FÍSICA

UNIVERSIDAD DE LA LAGUNA

NANOPEROVSKITE DOPED WITH Yb^{3+} AND Tm^{3+} IONS USED AS AN OPTICAL UPCONVERSION TEMPERATURE SENSOR

Autora

Laura García Rodríguez

Tutores

Inocencio Rafael Martín Benenzuela

Susana Ríos Rodríguez

Índice

Abstract

La dependencia con la temperatura de las bandas de emisión de la nanoperovskita $YAlO_3:Yb^{3+}/Tm^{3+}$ se ha analizado bajo una excitación de 975 nm con el objetivo de probar su eficiencia como sensor de temperatura. Entre las bandas de emisión de esta muestra, son de interés aquellas originadas por las transiciones $^3F_{2,3} \rightarrow {}^3H_6$ y $^3H_4 \rightarrow {}^3H_6$, localizadas en 700 y 800 nm respectivamente. Estas bandas tienen la ventaja de que pertenecen a la denominada primera ventana biológica del tejido humano, y además cumplen las condiciones óptimas para que exista una redistribución térmica de la población, pudiendo ser analizadas mediante la técnica conocida como "Fluorescence Intensity Ratio (FIR)".

El estudio de la dependencia con la temperatura de estas bandas se ha llevado a cabo mediante dos métodos diferentes basados en la ya nombrada técnica FIR, en un rango de temperaturas comprendido entre temperatura ambiente y 470 K. En cuanto al primer método, se han usado las áreas bajo ambas bandas de emisión; al haber redistribución térmica de la temperatura, estas bandas se poblarán de distinta manera en función de la temperatura a la que esté sometida la muestra, de manera que se puede obtener cómo depende la relación de intensidades entre las bandas con la temperatura. El segundo método se basa en el mismo principio, pero en vez de utilizar las bandas, se analizan las intensidades a dos longitudes de onda diferentes.

Un parámetro que caracteriza el rendimiento de nuestro sensor óptico es la sensitividad: ésta se define como la variación con la temperatura de la variable medida, que en este caso es la relación entre las intensidades de las bandas, que puede ser descrita por la ley de Boltzmann, relativa a su magnitud. Los resultados obtenidos muestran una mayor sensitividad en el rango biofísico de temperaturas con el primer método, mientras que, para temperaturas superiores a 340 K, la sensitividad es mayor con el segundo método.

Mediante la técnica FIR se consigue hacer una calibración, de manera que, conocido la relación entre las intensidades de las bandas, se puede saber la temperatura a la que está sometida la muestra, y viceversa. De esta manera, una vez hecha la calibración, podemos monitorizar la temperatura de la nanoperovskita en el rango de temperaturas mencionado anteriormente al ser calentada con un láser. Utilizando un láser de 975 nm y variando su potencia, se inducirá un cambio de temperatura en la muestra que podrá ser estimado conociendo la relación de intensidades entre las bandas bajo estudio.

Aim of this work

The main aim of this work is to study the viability of YAlO3:Yb3+/Tm3+ nanoperovskite as a thermal sensor. In order to achieve this goal, the characterization of the sample was carried out by means of the FIR technique, analysing the temperature variation of the emission bands of the mentioned nanoperovskite.

The specific objectives of this work can be summarized as follows:

- To analyze the upconversion mechanism in ytterbium and thulium ions which act as doping ions in the host matrix.

- To analyze the effect of thermalization on the emission spectrum of thulium ions using the "Fluorescence Intensity Ratio (FIR)" technique, and, therefore, perform a calibration of the optical sensor.

- To determine the best way to perform the FIR technique depending on the temperature range in which this work has been developed.

- To estimate the temperature of the sample under different excitation pump powers by using one of the previous calibration methods, and, therefore, to be able to control the temperature of the sample with the excitation source.

Chapter I: Introduction

Hoy en día, ha crecido el interés en los sensores ópticos debido a su alto rendimiento y a las numerosas ventajas que tienen en una gran cantidad de disciplinas diferentes. En este caso, el principal objetivo del trabajo se centra en estudiar la posibilidad de utilizar la nanoperovskita $YAlO_3:Yb^{3+}/Tm^{3+}$ como sensor óptico con la temperatura. Las elección de esta matriz y de estos dopantes en base a sus propiedades, hacen del conjunto un excelente candidato como sensor, además de despertar el interés en el campo de la medicina, ya que las bandas de emisión empleadas en el estudio caen dentro de la primera ventana biológica.

Temperature has always been one of the most important parameters to consider in a wide variety of scientific disciplines, such as engineering, astrophysics, chemistry or biology, among others [1,2]. Measuring temperature and being able to control it, has allowed new approaches to many fields, especially in medicine, in which the accurate detection and treatment of diseases is crucial [3,4]

Nowadays, optical temperature sensors based on the fluorescence intensity ratio (FIR) technique have attracted attention due to their accuracy and the new possibilities they allow [5,6]: the FIR technique provides a contactless method to measure temperature, since it consists on the comparison of two emission. These optical temperature sensors are composed of a laser as an excitation source, an optically active material which must be placed at the point of interest and a spectrometer as an optical detector.

Trivalent rare earths (RE^{3+}) present thermally coupled emitting levels, which means that the relative ion population of the former levels, and so their corresponding emissions, depend strongly on the temperature changes. This feature along with the excellent physico-chemical properties of RE^{3+} ions make them suitable as optically active materials [7].

For instance, ytterbium and thulium trivalent ions have been proved to be good candidates as probes to build this type of sensors due to their thermally coupled energy levels scheme [8, 9, 10]. Both $Yb^{3+}$and Tm^{3+}show absorption and emission bands that lie in the near-infrared window, where light penetrates better in human tissue. Moreover, Yb^{3+} has a great absorption cross section at 975 nm and transfers energy efficiently to thulium ions. On the other hand, the upconverted emission bands of thulium are appropriate for optical thermometry, because these emission bands lie in the first biological window. In the present work, Yb^{3+}/Tm^{3+}-codoped $YAlO_3$ nanoperovkite was studied in order to check its viability as temperature probe in the first biological window, taking advantage of the excellent physical and chemical properties of this matrix such as high hardness, good structural stability, and large mechanical strength. Moreover, in comparison with other matrix, $YAlO_3$ nanoperovkite has a low maximum phonon energy (around 650 cm^{-1} [11,12]), which makes it an excellent candidate as a host material for lanthanide ions [13, 14].

Chapter II: Theoretical background

En esta sección se abordarán los aspectos teóricos en los que se basa el procedimiento experimental y la obtención y análisis de los resultados de este trabajo. Así, se presentarán los fundamentos de la técnica FIR, en torno a la cual gira la mayor parte de este trabajo, lo que conlleva conocer qué niveles de energía pueden ser empleados, y se introducirán la sensitividad y la incertidumbre en la temperatura como parámetros de calidad a la hora de comparar el funcionamiento de los dos métodos de estimación de la temperatura, objeto de este estudio. Así, con las dos subsecciones que se detallan en este capítulo, sentaremos las bases a partir de las cuales se podrá llevar a cabo el trabajo propuesto.

2.1. Fluorescence Intensity Ratio technique (FIR)

The FIR technique consists on analysing the changes of the emission bands of RE^{3+} with temperature. This technique is only applicable to those transitions in which the energy gap of the energy levels is between 200 cm^{-1} and 2000 cm^{-1}, since this is the optimum range for the thermal redistribution of the population from the lower level to the upper one. If this gap is larger than 2000 cm^{-1}, the thermal energy (approximately k_BT) would not be able to promote electrons to the upper level, being this level extremely low populated. On the contrary, if the energy gap is lower than 200 cm^{-1}, the emissions from both levels would overlap, making it difficult to apply this technique [15].

Therefore, the ratio of the intensities depends on the temperature, but it is not affected by the pump power of the incident source, because the population of each level is proportional to this pump power.

Under low pump power of excitation, the intensity ratio between the emitting E_2 and E_3 levels, R, is described by Boltzmann's law, given by [16]:

$$R = \frac{I_{31}}{I_{21}} = \frac{\omega_{31}^{R} g_3 h\nu_3}{\omega_{21}^{R} g_2 h\nu_2} e^{\frac{-\Delta E}{K_B T}} = C e^{\frac{-\Delta E}{K_B T}} \quad (1)$$

where k_B is the Boltzmann constant, $\Delta E = E_3 - E_2$ is the energy gap between E_3 and E_2 thermalized levels, g_3 and g_2 are the degeneracies $(2J+1)$ of the levels, ω_{31}^{R} and ω_{21}^{R} are the spontaneous emission rates of the E_3 and E_2 levels to the ground level (E_1), respectively, and $h\nu_i$ is the average photon energy of each band. For the Tm^{3+} ions the thermalized levels correspond to the $^3F_{3,2}$ and $^3H_4$ levels (see Fig. 1).

If we determine the behaviour of the intensity ratio of two emission bands with temperature, the data can be fitted to Eq. (1) and parameters C and ΔE can be obtained.

Once the calibration is done, the temperature of the sample can be obtained by solving Eq. (1), obtaining [17]:

$$T = \left(\frac{-\Delta E}{K_B ln\left(\frac{R}{C}\right)} \right) \quad (2)$$

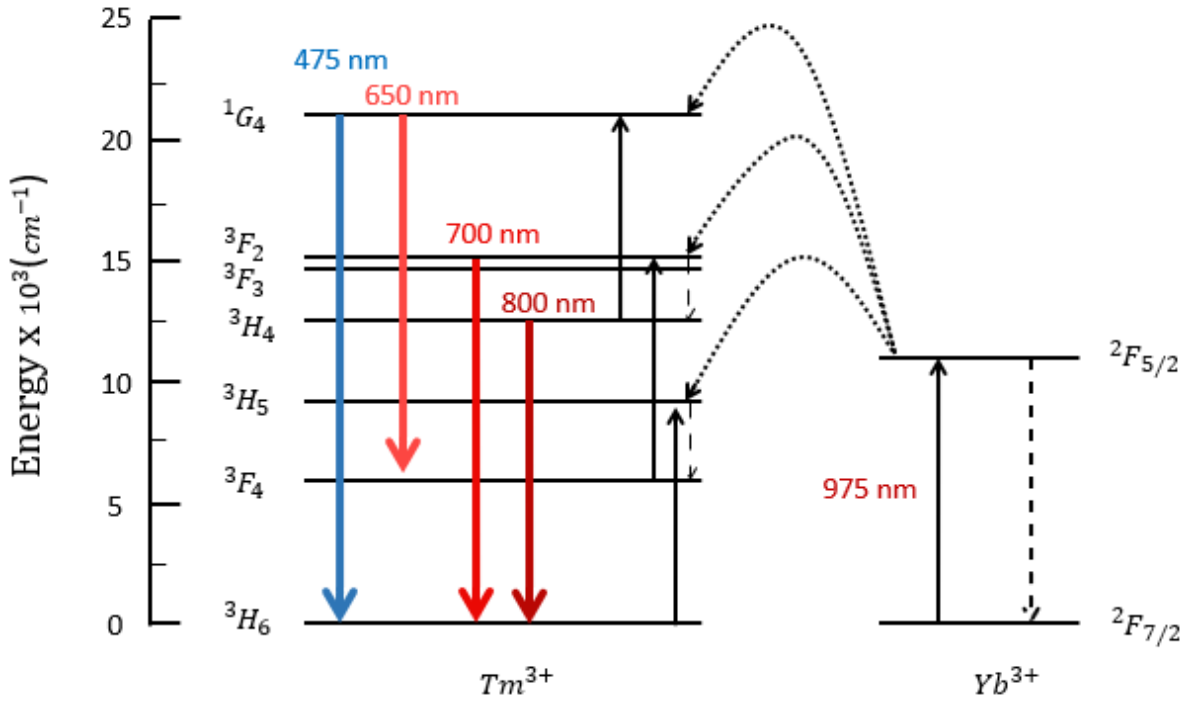

Fig. 1. Simplified energy level diagram of Tm3+and Yb3+ ions and possible upconversion mechanism under excitation at 975 nm. Black arrows represent photon excitation, black dashed curves represent energy transfer paths, black dashed lines arrows represent multiphonon relaxation processes, and colored arrows the radiative transition processes.

2.2. Sensitivity and temperature uncertainty

To characterise the performance of an optical temperature sensor, it's sensitivity will be considered. The sensitivity *S* of a certain optical temperature sensor is defined as the rate in which the measured parameter changes with temperature. In the particular case of an optical temperature sensor based on the FIR technique, this parameter is the intensity ratio and the sensitivity is defined as follows [16]:

$$S = \left|\frac{dR}{dT}\right| \tag{3}$$

However, in order to establish any comparison between the performance of different optical temperature sensors, the relative sensitivity, S_R is defined:

$$S_R = \frac{1}{R}\left|\frac{dR}{dT}\right| \tag{4}$$

and if the intensity ratio is characterized by a Boltzmann distribution (Eq. (1)) then the relative sensitivity can be expressed as:

$$S_R = \left(\frac{\Delta E}{K_B T^2}\right) \tag{5}$$

Therefore, in systems characterized by a Boltzmann distribution for the intensity ratio the relative sensitivity of the sensor only depends on the temperature and the energy gap between the thermally coupled levels. From this equation it is clear that as the energy gap increases, the relative sensitivity also does. However, this is true to some extent because a larger energy gap means that population of the upper level decreases and the emission intensity from this level is very low.

Moreover, the temperature uncertainty (or temperature resolution) can be obtained from [17]:

$$\delta T = \frac{\delta R}{S_R R} \tag{6}$$

Chapter III: Methodology and experimental procedures

En este capítulo se detallará la metodología seguida en cada procedimiento experimental y, posteriormente, se explicarán los distintos procedimientos experimentales que han permitido llevar a cabo la calibración del sensor óptico y la monitorización de la temperatura de la muestra, así como la propia síntesis de la nanoperovskita.

3.1. Methodology

When analysing the upconverted emission spectra of the $YAlO_3:Yb^{3+}/Tm^{3+}$ nanoperovskite, it can be noticed that the upconversion process is favoured when increasing the temperature of the sample. This can be explained as the 700 nm and 800 nm emission bands correspond to transitions which involve thermo-coupled energy levels that allow thermal redistribution of the population. Therefore, a calibration of the temperature sensor can be performed by determining the ratio between the aforementioned emission bands. In order to achieve this goal, the sample will be placed in a tubular furnace to heat the sample and obtain the corresponding spectra, and, therefore, the ratio as function of the temperature required for the calibration.

Once the calibration has been made, it can be possible to monitor the temperature of the sample for a given pump power excitation. This will be carried out by changing the pump power of the excitation source and analyzing the changes in the sample spectra. As the temperature is known for a given ratio, a relationship can be stablished between the pump power and the temperature of the sample.

3.2. Experimental procedures

3.2.1. Synthesis of nanoparticles

Nano-crystalline yttrium aluminium perovskite (YAP) of composition Y0.975Tm0.025Yb0.025AlO3 (YAP:Yb-Tm from now on) was obtained by the Pechini citrate sol–gel method in an air atmosphere. Stoichiometric molar ratios of high-purity precursor salts of Y(NO3)3·4H2O (ALDRICH, 99.9%), Al(NO3)3·9H2O (ALDRICH, 99.9%), Tm(NO3)3·5H2O (ALDRICH, 99.9%) and $Yb(NO_3)_3 \cdot 5H_2O$ (ALDRICH, 99.9%) materials were mixed and dissolved in 25 ml of 1 M HNO3 and then stirred for three hours at a temperature of 353 K. Citric acid, with a molar ratio of metal ions to citric acid of 1:2, was later added to the solution, which was stirred and heated at 363 K until reaching the transparency of the solution. Afterwards, 4 mg of polyethylene glycol was added to the solution, helping to create a gel that was annealed at 673 K for six hours in order to remove the residual nitrates and organic compounds. The resulting powder sample was finally annealed out at 1473 K for twenty hours. Then, the sample was given a second thermal treatment at 1823 K for twelve hours. The outcome obtained is chemically stable.

Powder X-ray diffraction data were collected on a PANalytical X'Pert PRO diffractometer (Bragg-Brentano geometry) with an X'Celerator detector employing the Cu Kα1 radiation (λ=1.5405 Å) in the angular range $5º < 2\Theta < 80º$, by continuous scanning with a step size of 0.02º, achieving the orthorhombic phase in the sample as well as the crystallite size around 40 nm reported in previous works working with the same host material with others lanthanide ions [11, 18]. In addition, TEM image of the same host matrix undoped and doped with another lanthanide ion was reported, showing the morphology of such nanomaterial [19].

3.2.2. Optical measurements

The luminescence measurements were performed from room temperature (RT) up to 470K in a tubular furnace, where a thermocouple was placed to read the exact temperature of the sample. The excitation of the sample was carried out with a 975 nm diode laser, which was collimated by a lens (f=75mm) and then focused with a second lens (f=200 mm) placed so that its back focal point is just in the centre of the furnace, where the sample was located.

It should be noticed that the power density at which the temperature calibration was made about 8.0 W/cm^2 in order to avoid the heating of the sample.

The luminescence from the sample was focalized at the tip of an optical fiber located in the opposite side of the furnace with a 60 mm focal length lens. Before being focused, the emission was collimated with a lens (f=200 mm), and then filtered with an 800 nm short pass filter. The optical fiber was coupled to a single grating CCD spectrometer (Andor SR-3031-B CCD Newton DU920N). The heating of the sample was performed at a rate of 0.83 K/min, from RT to 470 K, and the detection was carried out with a resolution of 0.7 nm and an integration time of 10 s. This experiment allowed to calibrate the optical sensor with temperature.

Once the optical sensor was calibrated with temperature, it was possible to monitor the temperature of the nanoperovskite from RT to 430 K by heating the sample with the laser excitation source. The excitation intensity at 975 nm was varied changing the pump power of the laser. The Gaussian beam was focused in the sample with a 75 mm lens and the waist spot size on the sample (defined as the $1/e^2$ radius of the intensity) was 50x50 μm^2. Then, the emission was focused on the tip of an optical fiber with a 50 mm focal length lens, previously filtered by an 800 nm short pass filter and recorded by the same spectrometer used in the calibration procedure of the optical sensor.

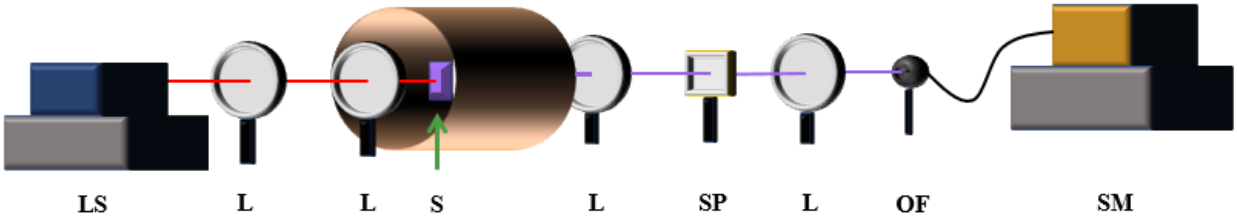

Fig. 2. Experimental set-up used for the temperature calibration. The acronym labels correspond to LS Laser Source (975 nm), L Lens, S Sample, SP Short Pass Filter, OF Optical Fiber and SM Spectrometer.

Chapter IV: Results and discussion

En este capítulo se presentarán y se discutirán los resultados obtenidos durante el trabajo. En primer lugar, se ha obtenido el espectro de emisión de la muestra. En este espectro se observan las bandas correspondientes a las transiciones $^3F_{2,3} \rightarrow {}^3H_6$ *and* $^3H_4 \rightarrow {}^3H_6$*, que se demuestra que son óptimas para ser usadas en la determinación de la temperatura.*

En cuanto a la calibración del sensor, los resultados muestran una sensitividad mayor en el rango biofísico de temperaturas cuando utilizamos las bandas centradas en 700 nm y 800 nm en la técnica FIR que cuando utilizamos los intensidades a 690 nm y 815 nm. Sin embargo, para temperaturas superiores a 340 K, este segundo método presenta una mayor sensitividad que el primero. Así, la sensitividad relativa SR1 alcanza su máximo de 0.019 K^{-1} *para una temperatura de 293 K, mientras que el máximo de 0.014* K^{-1} *de la sensitividad relativa SR2 se obtiene para una temperatura de 340 K.*

Las incertidumbres de las ratios de intensidades varían desde 1% (T=300 K) a 4% (T=470 K) para el primer método de calibración, y de 2.6% (T=300 K) a 0.6% (T=470) para el segundo método. En cuanto a la incertidumbre en la temperatura, se obtiene una variación de 0.5 K (T=300 K) a 5 K (T=470 K) para el primer método de calibración, y de 2 K (T=300 K) a 0.7 K (T=470 K) para el segundo método.

Por último, se analiza la variación del espectro de la muestra con la potencia de bombeo de la fuente de excitación, de manera que se

obtiene una curva que relaciona dicha potencia con la temperatura de la muestra.

4.1. Upconversion emission

The emission spectrum of the YAP:Yb-Tm nanocrystal at room temperature excited at 975 nm is shown in Fig. 3. The emission bands centered at 475, 650, 700 and 800 nm are assigned to the $^1G_4 \rightarrow {}^3H_6$, $^1G_4 \rightarrow {}^3F_4$, $^3F_{2,3} \rightarrow {}^3H_6$ and $^3H_4 \rightarrow {}^3H_6$ transitions, respectively. As it is known, in systems codoped with Yb^{3+}-Tm^{3+}, the $^1G_4$ level of the thulium is populated by an upconversion process of three photons, and the $^3H_4$ level is populated by an upconversion process of two photons [20]. This upconversion mechanism is depicted in Fig. 1. The Yb^{3+} ions absorb laser photons as they have a great absorption cross section at 975 nm. Therefore, one excited Yb^{3+} ion excites the ground state of the Tm^{3+} to the $^3H_5$ state. Then, due to its proximity, the $^3F_4$ state of the Tm^{3+} ions is populated by multiphonon relaxation processes. A second energy transfer process from another excited Yb^{3+} ion populates the $^3F_{2,3}$ state of Tm^{3+} ions, which generates the 700 nm emission band. Moreover, nonradiative relaxation from $^3F_{2,3}$ cause the population of the $^3H_4$ state of Tm^{3+} ions, resulting in the 800 nm emission band [21]. Finally, a third transfer from Yb^{3+} to the $^3H_4$ state populates the $^1G_4$ level.

The inset of Fig.3, shows the dependence of the upconversion (UC) emission intensities with the excitation power, being *n* the number of absorbed photons per UC emitted photon. As it has been explained, *n* values close to 2 and 3 are expected for the 800 and 475 nm emission bands respectively, but as can be seen in Fig. 3 lower values were obtained [22]. This fact could be related to saturation effects of the Yb^{3+} and the first excited state of Tm^{3+} [23].

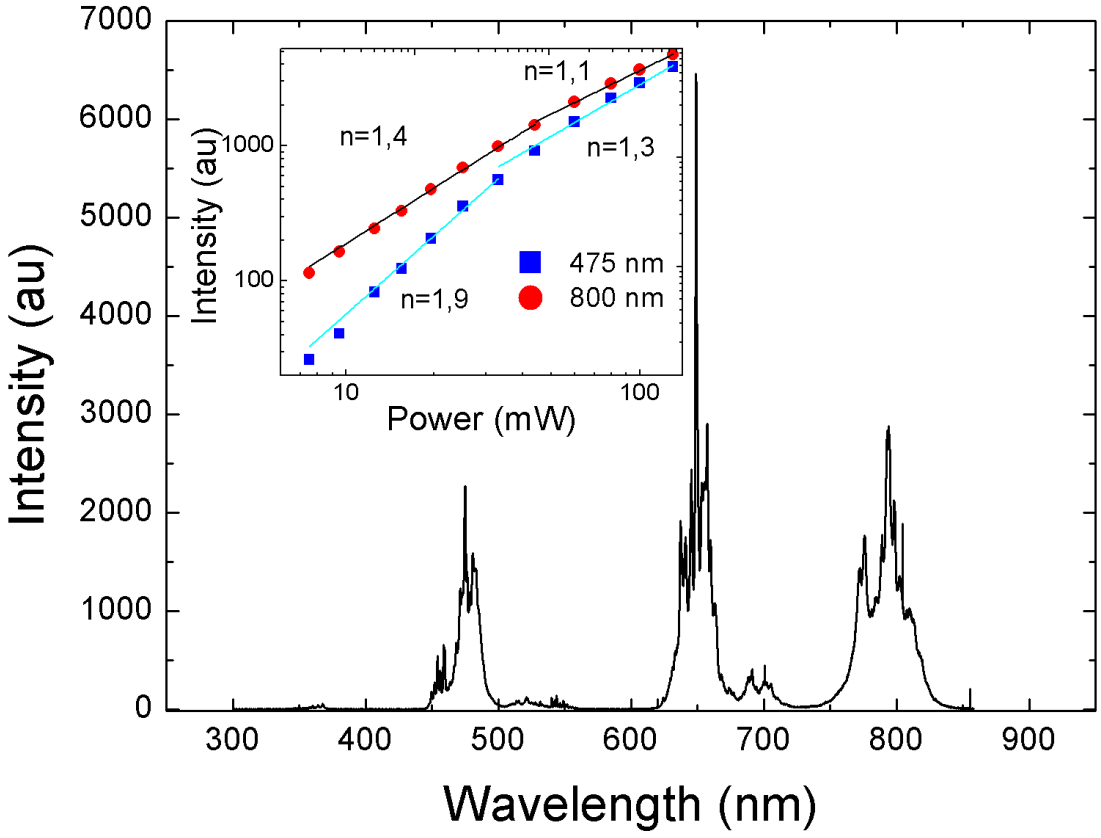

Fig. 3. Room-temperature upconversion emission spectrum of the YAP:Yb-Tm nanocrystals obtained under a pump power of 80 mW at 975 nm. The inset shows the dependence of the upconversion emission with the excitation power in a logarithmic scale.

The emission bands at 700 nm ($^3F_{2;3}\rightarrow {}^3H_6$) and 800 nm ($^3H_4\rightarrow {}^3H_6$) are proved to be appropriate for optical temperature sensing, because $^3F_{2,3}$ and $^3H_4$ energy levels are thermally coupled [24]. Fig. 4 shows the 700 and 800 nm emission bands for two different temperatures. It can be seen that the intensity of the 700 nm emission band increases with temperature, while the 800 nm emission band remains quite constant with temperature. This fact is due to the thermally population described before.

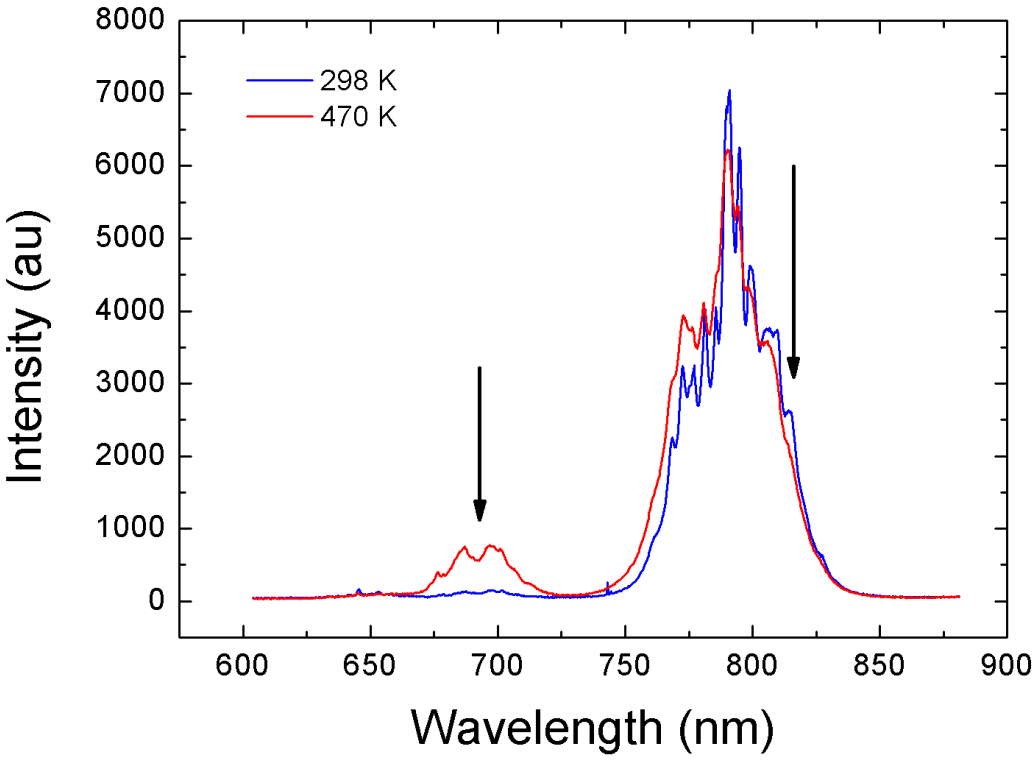

Fig. 4. Luminescence spectra for two different temperatures under 975 nm diode laser excitation. The arrows show the peaks used in the second method of the FIR technique: 690 and 815 nm respectively.

4.2. Calibration methods

In this section, two different calibration procedures based in the FIR technique were considered.

The first one consists on the determination of the emission intensities by the integration of each band. The ratio of these bands (R_1) is described by the Boltzmann distribution according to Eq. (1) and it is shown in Fig 5. Fitting the experimental ratios to an exponential function, the values C= 1.94 and ΔE=1173 cm^{-1} have been obtained. The relative sensitivity S_{R1} was calculated according to Eq. (5), being 0.019 K^{-1} the maximum value of this magnitude at 293 K (see Fig. 5). S_{R1} is related to intensity ratios modelled by Eq.(1) and is given by $\Delta E/KT^2$. The YAP produce a high splitting among the $^3F_{2,3}$ and $^3H_4$ levels and consequently a high value for the relative thermal sensitivity.

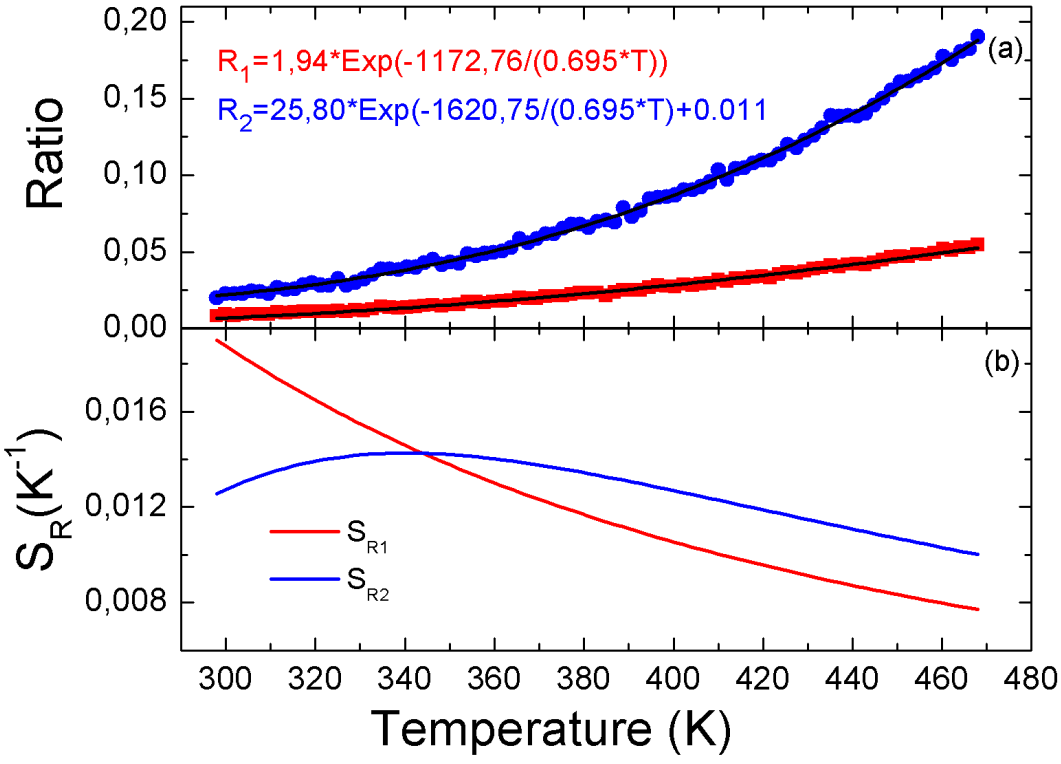

Fig. 5. Fluorescence intensity ratios (a) and relative sensitivities (b) for the two calibration methods as function of the temperature in the range of 298-470 K.

Other works have explored the possibility to predict the calibration curve in this first calibration using other methods [25]. Assuming that for a low enough excitation pump power there is no laser heating effect and the temperature of the sample is T_0. Then when the sample is heated the temperature can be obtained using Eq.(1) by [25]:

$$\frac{1}{T} = \frac{1}{T_0} + \frac{K_B}{\Delta E} ln\left(\frac{R}{R_0}\right) \quad (7)$$

As it can be seen, it is not necessary to know the value of the constant C to determine the absolute temperature. However, the value of ΔE needs to be calculated, as example, using the absorption spectra. This energy gap between the thermalized energy levels can be estimated from the spectral positions of the centroids of the absorption bands corresponding to the transitions between the thermalized energy levels. In this way a value of 1776 cm^{-1} has been obtained and it is not in very good agreement with the value of 1173 cm^{-1} (obtained from fitting procedure). This discrepancy can be explained in basis to the Stark sub-levels that are observed in each band. In other previous works have been also different concordances among the ΔE values obtained from the absorption bands or from the fitting procedure (see Table 2 in Ref. [26]).

Concerning the second calibration procedure, the ratio of two spectra recorded at low and high temperatures was obtained and it is shown in Fig. 6. It can be seen that the maximum and minimum rates were found at about 690 and 815 nm, and so these wavelengths were selected to study their intensity ratio versus temperature. The ratio (R_2) calculated by this method can be described according to the Boltzmann's law plus a constant (D) as it is shown in Fig. 5.

The use of an additional constant in Eq. (1) for this second method is justified considering that at 690 nm, there is a little contribution of the emission centered at 650 nm. Therefore, in order to improve this effect, the constant D was added (see Ref. [17]).

From this calibration procedure, the values C=25.80 and ΔE=1621 cm^{-1} and the additional constant D=0.0112 have been obtained. The relative sensitivity S_{R2} reaches a maximum value of 0.014 K^{-1} at 340 K (see Fig. 5).

According to Fig. 5, the first calibration procedure is better in the range between RT up to 340 K, while the second one is better in the range between 340 and 470 K.

In Table 1, a comparison of the values of the relative sensitivity obtained for other nanocrystals doped with rare earth ions is presented. From this table and the relative sensitivities shown in Fig. 5b, it can be concluded that YAP:Yb-Tm reaches a maximum value of the relative sensitivity in the physiological range which is higher than the values obtained in other rare earth doped nanocrystals.

As can be seen in Fig. 5b, a combination of the two calibration methods R_1 and R_2 leads to a relative sensitivity larger than 10^{-2} K^{-1} in the range between 340 and 470 K.

The intensity ratios and temperature uncertainties were estimated for both calibration methods by using the procedure described in Ref. [17]. The intensity ratio uncertainties range from 1% (T=300 K) to 4% (T=470 K) for the calibration 1 and from 2.6% (T=300 K) to 0.6% (T=470) for the calibration 2.

Respect to temperature uncertainties, we have evaluated Eq. (6) obtaining values ranging from 0.5 K (T=300 K) to 5 K (T=470 K) for the calibration 1. On the other hand, for the calibration 2 the uncertainties vary from 2 K (T=300 K) to 0.7 K (T=470 K).

We can conclude that if we combine both combination procedures the temperature uncertainty can be kept below 1 K in all the temperature range (300-470 K).

It can be seen in Fig. 5a, that small oscillations appear in R2 as compared with R1. These small oscillations can be produced by peaks shifts or splitting of energy sublevels that change with the temperature. Nevertheless, the values of these oscillations are in the range of the uncertainties previously estimated.

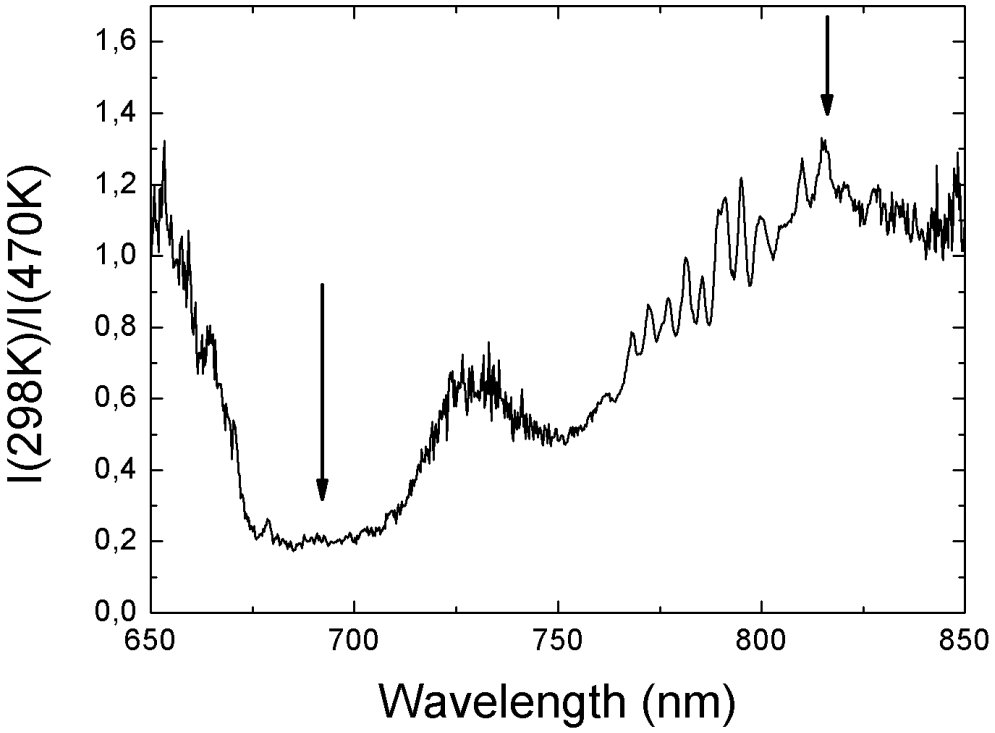

Fig. 6. Ratio of upconversion spectra obtained at two different temperatures (298 and 470 K). The wavelengths used for the second calibration method R2 are marked with arrows.

Table 1. Maximum relative sensitivity for different RE^{3+} temperature optical sensors in the physiological range

Optical sensor	λ range (nm)		Temp. range (K)	λ_{Exc} (nm)	Maximum S_{REL} within the physiological range (303-318 K) ($x10^{-3}$ K^{-1})	Ref.
	Upper energy level	Lower energy level				
YAP:Yb-Tm (nano)	675-725	750-825	298-470	975	18 (R_1)	This work
	690	815	298-470	975	14 (R_2)	
YAP:Tm (nano)	792-800	800-803	294-324	1210	10	[8]
$Na_2Y_2B_2O_7$: Er^{3+}/Yb^{3+} nano-phosphor	510-536	538-572	300-613	980	8.3	[20]
$CaMoO_4$: Er^{3+}/Yb^{3+} nano-phosphor	517-542	543-578	300-535	980	5.9	[21]
CaF_2: Tm/Yb (nano)	785-795	795-805	299-323	920	2.4	[22]
$LiNdP4O_{12}$ (nano)	880-890	890-920	250-500	808	2.3	[23]
$NaYF_4$: Nd (nano)	860-864	865-880	273-423	830	1.3	[24]
YAG: Nd (nano)	935-941	943-950	283-343	808	1.2	[25]
LaF_3: Nd (nano)	855-874	875-890	283–333	808	1	[26]

4.3. Laser heating

The previous calibration processes have been made by exciting the sample with a low pump power in order to do not heat the sample. It must be taken into account that nonradiative processes that involve emission phonons can produce heating of the matrix. In some experiments, however, it is interesting to control the temperature of the sample by changing the excitation pump power. Therefore, the upconversion emission spectra for excitation at 975 nm and different powers were recorded and the temperature of the sample was estimated using the calibration method R_2.

Considering the experimental conditions detailed in the experimental section, the sample absorbed around 50% of the 186 mW excitation power, achieving a temperature around 430 K.

In Fig. 7 both the measurements of the ratio of intensities for different values of the laser power and the inferred temperature values are presented in the heating and cooling processes. It can be seen that a good agreement in the values has been obtained for both procedures. Thus, with this technique the sample temperature can be properly monitored in the range from 300 to 430 K.

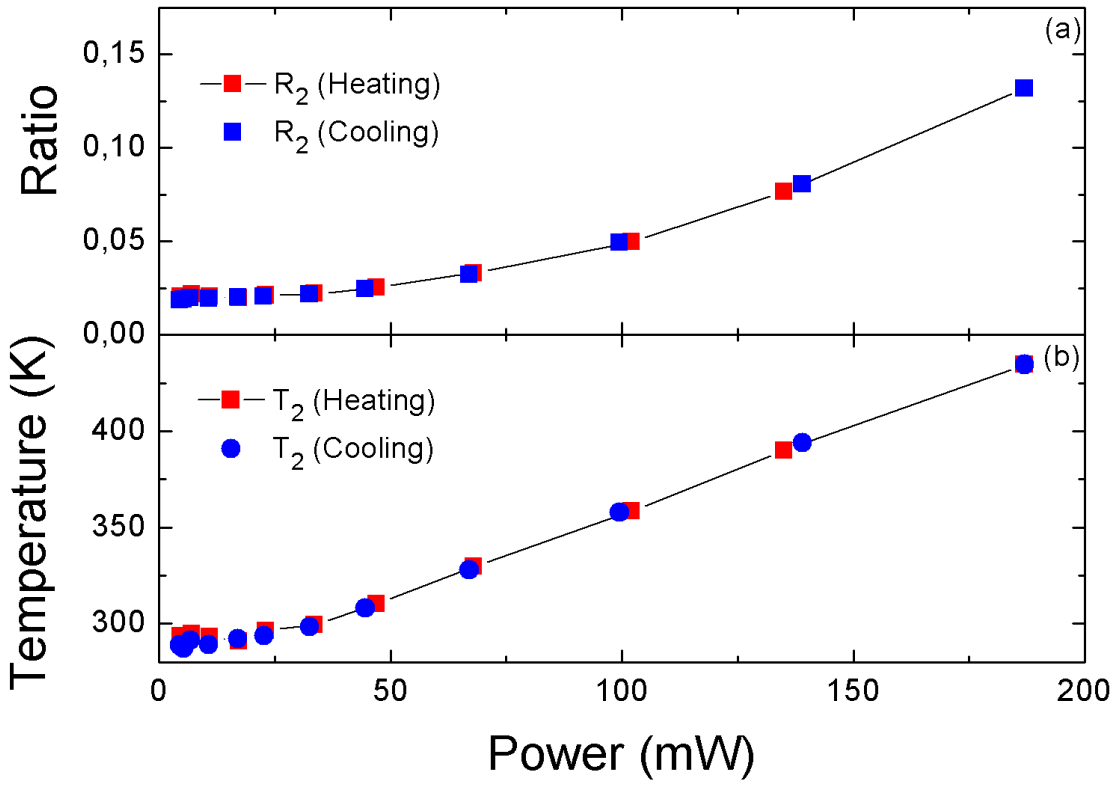

Fig. 7. Intensities ratios (a) and temperature induced (b) obtained by R1 and R2 methods on the sample by the laser heating as a function of the pump power. Both heating and cooling processes are shown.

Chapter V: Conclusions and future projects

The thermal sensing capability of the YAP:Yb-Tm was studied in order to check its viability as an optical temperature sensor.

Two different calibration procedures based in the FIR technique were carried out, resulting in two different relative sensitivities: S_{R1} reaches a maximum value of 0.019 K^{-1} at the lowest temperature, while S_{R2} reaches a maximum value of 0.014 K^{-1} at 340 K. The conventional FIR technique (R_1) has its better sensitivity in the range from RT to 340 K, and the second method here proposed (R_2) performs better from 340 to 470 K. If a combination of both methods is used, the relative sensitivity will stay above 10^{-2} K in the whole temperature range.

In addition, the laser induced heating effect in YAP:Yb-Tm has been studied, and the temperature of the sample has been estimated in the heating and cooling process, obtaining a good agreement between them. These features confirm the potential utility of YAP:Yb-Tm as an optical thermal sensor for biological applications.

References

[1] G. Adam, J. Gibbs, J. Chem. Phys. 43 (1965) 139.

[2] H. Pörtner, Comp. Biochem. Physiol. A Mol. Integr. Physiol. 132 (2002) 739.

[3] B. Rubinsky, G. Onik, Int. J. Refrig. 14 (1991) 190.

[4] D. Needham, M. Dewhirst, Adv. Drug Deliv. Rev. 53 (2001) 285

[5] Y. Zhou, F. Qin, Y. Zheng, Z. Zhang, W. Cao, Opt. Lett. 40 (2015) 4544.

[6] S. Zhou, X. Li, X. Wei, C. Duan, M. Yin, Sens. Actuators. B. Chem. 231 (2016) 641

[7] V. Rai, S. Rai, Spectrochim. Acta. A. Mol. Biomol. Spectrosc. 68 (2007) 1406.

[8] M. Hernández-Rodriguez, A. Lozano-Gorrín, V. Lavín, U. Rodríguez-Mendoza, I. Martín, Opt. Express 25 (2017) 27845.

[9] L. Xing, Y. Xu, R. Wang, W. Xu, Z. Zhang, Opt. Lett. 39 (2014) 454.

[10] A. Pereira, K. Kumar, W. Silva, W. Santos, D. Jaque, C. Jacinto, Sens. Actuators B. Chem. 213 (2015) 65.

[11] M.A. Hernández-Rodríguez, V. Monteseguro, A.D. Lozano-Gorrín, F.J. Manjón, J. González-Platas, P. Rodríguez-Hernández, A. Muñóz, V. Lavín, U.R. Rodríguez- Mendoza, J. Phys. Chem. C. 121 (2017) 15353.

[12] M.S. Marques, L.D.S. Menezes, W. Lozano B, L.R.P. Kassab, C.B. De Araújo, J. Appl. Phys. 113 (2013) 053102.

[13] R. Moncorgé, B. Chambon, J. Y. Rivoire, N. Garnier, E. Descroix, P. Laporte, H. Guillet, S. Roy, J. Mareschal, D. Pelenc, J. Doury, P. Farge, Opt. Mater. 8 (1997) 109

[14] M. Weber, M. Bass, K. Andringa, R. Monchamp, E. Comperchio, Appl. Phys. Lett. 15 (1969) 342.

[15] V. Rai, Appl. Phys. B. 88 (2007) 297.

[16] S. Wade, S. Collins, G. Baxter, J. Appl. Phys. 94 (2003) 4743.

[17] Brites, C. D. S.; Millan, A.; Carlos, L. D. Lanthanides in luminescent thermometry, in: J.V.G. Bünzli, V.K. Pecharsky (Eds.), Handbook on the Physics Chemistry of the Rare Earths: Including Actinides, Elsevier B.V., Amsterdam, 2016: pp. 339–427.

[18] M.A. Hernández-Rodríguez, A.D. Lozano-Gorrín, I.R. Martín, U.R. Rodríguez-Mendoza, V. Lavín, J. Lumin. 188 (2017) 204.

[19] M.A. Hernández-Rodríguez, A.D. Lozano-Gorrín, I.R. Martín, U.R. Rodríguez-Mendoza, V. Lavín, Sensors Actuators, B Chem. 255 (2018) 970.

[20] K. Kumar, W. Silva, K. Venkata Krishnaiah, C. Jayasankar, C. Jacinto, J. Nanophotonics 8 (2014) 083093.

[21] D. Simpson, W. Gibbs, S. Collins, W. Blanc, B. Dussardier, G. Monnom, P. Peterka, G. Baxter, Opt. Express 16 (2008) 13781.

[22] M. Pollnau, D. Gamelin, S. Lüthi, H. Güdel, M. Hehlen, Phys. Rev., B Condens. Matter. 61 (2000) 3337.

[23] C. Jacinto, M. Vermelho, E. Gouveia, M. de Araujo, P. Udo, N. Astrath, M. Baesso, Appl. Phys. Lett. 91 (2007) 071102.

[24] W. Xu, X. Gao, L. Zheng, Z. Zhang, W. Cao, Sens. Actuators B, 173 (2012) 250.

[25] S. Balabhadra, M. L. Debasu, C. D. S. Brites, R. A. S. Ferreira, L. D. Carlos, J. Phys. Chem. C 121 (2017) 13962.

[26] W. Xu, D. Li, H. Hao, Y. Song, Y. Wang, X. Zhang, Optical Materials, 78 (2018) 8.

[27] A. Soni, V. Rai, M. Mahata, Mater. Res. Bull. 89 (2017) 116.

[28] S. Sinha, M. Mahata, K. Kumar, S. Tiwari, V. Rai, Spectrochim. Acta. A. Mol. Biomol. Spectrosc. 173 (2016) 369.

[29] N. Dong, M. Pedroni, F. Piccinelli, G. Conti, A. Sbarbati, J. Ramírez-Hernández, L. Maestro, M. Iglesias-de la Cruz, F. Sanz-Rodriguez, A. Juarranz, F. Chen, F. Vetrone, J. Capobianco, J. Solé, M. Bettinelli, D. Jaque, A. Speghini, ACS Nano, 5 (2011) 8665.

[30] L. Marciniak, K. Prorok, A. Bednarkiewicz, A. Kowalczyk, D. Hreniak, W. Strek, J. Lumin. 176 (2016) 144.

[31] D. Wawrzynczyk, A. Bednarkiewicz, M. Nyk, W. Strek, M. Samoc, Nanoscale 4 (2012) 6959.

[32] A. Benayas, B. del Rosal, A. Pérez-Delgado, K. Santacruz-Gómez, D. Jaque, G. Hirata, F. Vetrone, Adv. Opt. Mater. 3 (2015) 687.

[33] U. Rocha, C. Jacinto Da Silva, W. Ferreira Silva, I. Guedes, A. Benayas, L. Martínez Maestro, M. Acosta Elias, E. Bovero, F.C.J.M. Van Veggel, J.A. García Solé, D. Jaque, ACS Nano 7 (2013) 1188.

Appendix

In this section it will be attached the uncorrected proof copy of the article "Nanoperovskite doped with Yb^{3+} and Tm^{3+} ions used as an optical upconversion temperature sensor" recently published in *Optical Materials* in pages 187-191 of the volume 83 (https://doi.org/10.1016/j.optmat.2018.06.009).

Optical Materials xxx (2018) xxx-xxx

Contents lists available at ScienceDirect

Optical Materials

journal homepage: www.elsevier.com

Nanoperovskite doped with Yb^{3+} and Tm^{3+} ions used as an optical upconversion temperature sensor

L. Garc a-Rodr guez[a], L. de Sousa-Vieira[a], M.A. Hern ndez-Rodriguez[a], A.D. Lozano-Gorr n[a], V. Lav n[a, b], U.R. Rodr guez-Mendoza[a, c], J. Gonz lez-Platas[a], S. R os[a], I.R. Mart n[a, c,]

[a] Departamento de F sica, Universidad de La Laguna, Apdo. 456, E-38200, San Crist bal de La Laguna, Santa Cruz de Tenerife, Spain
[b] Instituto Universitario de Estudios Avanzados en F sica, At mica y Fot nica (IUdEA), Universidad de La Laguna, Apdo. 456, E-38200, San Crist bal de La Laguna, Santa Cruz de Tenerife, Spain
[c] Instituto Universitario de Materiales y Nanotecnolog a (IMN), Universidad de La Laguna, Apdo. 456, E-38200, San Crist bal de La Laguna, Santa Cruz de Tenerife, Spain

ARTICLE INFO

Keywords:
Nanoperovskite
Upconversion
Thermal sensor
Relative sensitivity

ABSTRACT

The temperature variation of the emission bands of the $YAlO_3$:Yb^{3+}/Tm^{3+} nanoperovskite has been analysed under 975 nm excitation to test its performance as a temperature sensor. The emission bands, originating from $^3F_{2,3}$ $^3H_6$ and $^3H_4$ $^3H_6$ transitions, are located at 700 and 800 nm respectively (first biological window of the human tissue), and were measured from room temperature until 470 K. The calibration of the optical sensor has been made by two different methods. In the first one, based on the fluorescence intensity ratio technique, the areas under the two emission bands were used. In the second procedure the ratio of the intensities at two different wavelengths is estimated. The results showed a higher sensitivity in the biophysical temperature range for the fluorescence intensity ratio method, while a better sensitivity was obtained with the second method for temperatures above 340 K. Once the calibration is made, it is possible to monitor the temperature of the nanoperovskite in the aforementioned range while the sample is heated with the laser.

1. Introduction

Temperature has always been one of the most and important parameters to consider in a wide variety of scientific disciplines, such as engineering, astrophysics, chemistry or biology, among others [1,2]. Measuring temperature and being able to control it, has allowed new approaches to many fields, especially in medicine, in which the accurate detection and treatment of diseases is crucial [3,4].

Nowadays, optical temperature sensors based on the fluorescence intensity ratio (FIR) technique have attracted attention due to their accuracy and the new possibilities they allow [5,6]: the FIR technique provides a contactless method to measure temperature, since it consists on the comparison of two emission. These optical temperature sensors are composed of a laser as an excitation source, an optically active material which must be placed at the point of interest and a spectrometer as an optical detector.

Trivalent rare earths (RE^{3+}) present thermally coupled emitting levels, which means that the relative ion population of the former levels, and so their corresponding emissions, depend strongly on the temperature changes. This feature along with the excellent physico-chemical properties of RE^{3+} ions make them suitable as optically active materials [7].

For instance, ytterbium and thulium trivalent ions have been proved to be good candidates as probes to build this type of sensors due to their thermally coupled energy levels scheme [8 10]. Both Yb^{3+} and Tm^{3+} show absorption and emission bands that lie in the near-infrared window, where light penetrates better in human tissue. Moreover, Yb^{3+} has a great absorption cross section at 975 nm and transfers energy efficiently to thulium ions. On the other hand, the upconverted emission bands of thulium are appropriate for optical thermometry, because these emission bands lie in the first biological window. In the present work, Yb^{3+}/Tm^{3+} codoped $YAlO_3$ nanoperovkite was studied in order to check its viability as temperature probe in the first biological window, taking advantage of the excellent physical and chemical properties of this matrix such as high hardness, good structural stability, and large mechanical strength. Moreover, in comparison with other matrix, $YAlO_3$ nanoperovkite has a low maximum phonon energy (around 650 cm^{-1} [11,12]), which makes it an excellent candidate as a host material for lanthanide ions [13,14].

Corresponding author. Departamento de F sica, Universidad de La Laguna, Apdo. 456, E-38200, San Crist bal de La Laguna, Santa Cruz de Tenerife, Spain.
Email address: imartin@ull.es (I.R. Martín)

https://doi.org/10.1016/j.optmat.2018.06.009
Received 15 March 2018; Received in revised form 24 May 2018; Accepted 5 June 2018
Available online xxx
0925-3467/

2. Theoretical background

2.1. Fluorescence intensity ratio technique (FIR)

The FIR technique consists on analysing the changes of the emission bands of RE^{3+} with temperature. This technique is only applicable to those transitions in which the energy gap of the energy levels is between 200 cm^{-1} and 2000 cm^{-1}, since this is the optimum range for the thermal redistribution of the population from the lower level to the upper one. If this gap is larger than 2000 cm^{-1}, the thermal energy (approximately k_BT) would not be able to promote electrons to the upper level, being this level extremely low populated. On the contrary, if the energy gap is lower than 200 cm^{-1}, the emissions from both levels would overlap, making it difficult to apply this technique [15].

Therefore, the ratio of the intensities depends on the temperature, but it is not affected by the pump power of the incident source, because the population of each level is proportional to this pump power.

Under low pump power of excitation, the intensity ratio between the emitting E_2 and E_3 levels, R, is described by Boltzmann s law, given by Ref. [16]:

$$R = \frac{I_{31}}{I_{21}} = \frac{\omega_{31}^R g_3 h\nu_3}{\omega_{21}^R g_2 h\nu_2} e^{\frac{-\Delta E}{K_B T}} = Ce^{\frac{-\Delta E}{K_B T}} \quad (1)$$

where k_B is the Boltzmann constant, $E = E_3 \quad E_2$ is the energy gap between E_3 and E_2 thermalized levels, g_3 and g_2 are the degeneracies $(2J + 1)$ of the levels, ω_{31}^R and ω_{21}^R are the spontaneous emission rates of the E_3 and E_2 levels to the ground level (E_1), respectively, and h $_i$ is the average photon energy of each band. For the Tm^{3+} ions the thermalized levels correspond to the $^3F_{3,2}$ and $^3H_4$ levels (see Fig. 1).

If we determine the behaviour of the intensity ratio of two emission bands with temperature, the data can be fitted to Eq. (1) and parameters C and E can be obtained.

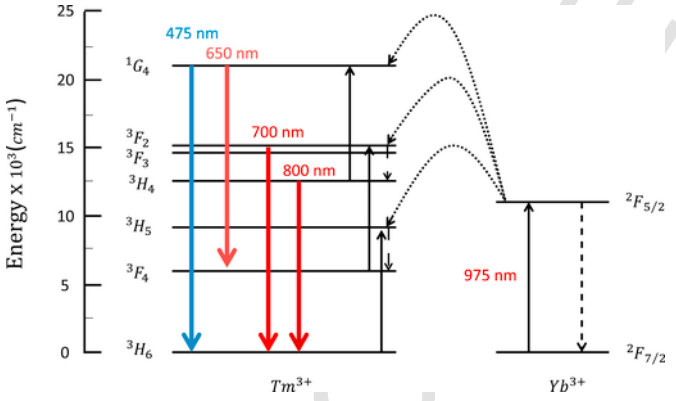

Fig. 1. Simplified energy level diagram of Tm^{3+} and Yb^{3+} ions and possible upconversion mechanism under excitation at 975 nm. Black arrows represent photon excitation, black dashed curves represent energy transfer paths, black dashed lines arrows represent multiphonon relaxation processes, and colored arrows the radiative transition processes.

Once the calibration is done, the temperature of the sample can be obtained by solving Eq. (1), obtaining [17]:

$$T = \left(\frac{-\Delta E}{K_B ln\left(\frac{R}{C}\right)} \right) \quad (2)$$

2.2. Sensitivity

To characterise the performance of an optical temperature sensor, it s sensitivity will be considered. The sensitivity S of a certain optical temperature sensor is defined as the rate in which the measured parameter changes with temperature. In the particular case of an optical temperature sensor based on the FIR technique, this parameter is the intensity ratio and the sensitivity is defined as follows [16]:

$$S = \left| \frac{dR}{dT} \right| \quad (3)$$

However, in order to establish any comparison between the performance of different optical temperature sensors, the relative sensitivity, S_R is defined:

$$S_R = \frac{1}{R} \left| \frac{dR}{dT} \right| \quad (4)$$

and if the intensity ratio is characterized by a Boltzmann distribution (Eq. (1)) then the relative sensitivity can be expressed as:

$$S_R = \left(\frac{\Delta E}{K_B T^2} \right) \quad (5)$$

Therefore, in systems characterized by a Boltzmann distribution for the intensity ratio the relative sensitivity of the sensor only depends on the temperature and the energy gap between the thermally coupled levels. From this equation it is clear that as the energy gap increases, the relative sensitivity also does. However, this is true to some extent because a larger energy gap means that population of the upper level decreases and the emission intensity from this level is very low. Moreover, the temperature uncertainty (or temperature resolution) can be obtained from Ref. [17]:

$$\delta T = \frac{\delta R}{S_R R} \quad (6)$$

3. Experimental

3.1. Synthesis of nanoparticles

Nano-crystalline yttrium aluminum perovskite (YAP) of composition Y0.975Tm0.025Yb0.025AlO3 (YAP:Yb-Tm from now on) was obtained by the Pechini citrate sol gel method in an air atmosphere. Stoi-

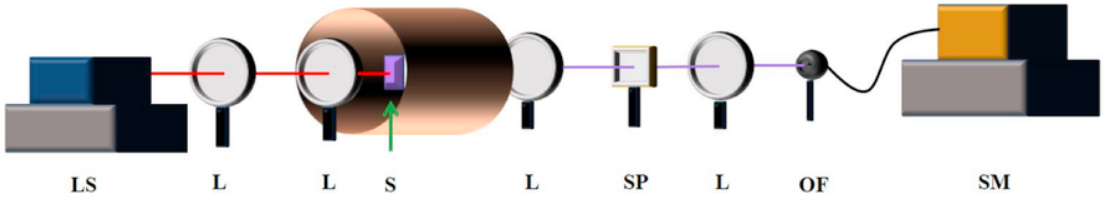

Fig. 2. Experimental set-up used for the temperature calibration. The acronym labels correspond to **LS** Laser Source (975 nm), **L** Lens, **S** Sample, **SP** Short Pass Filter, **OF** Optical Fiber and **SM** Spectrometer.

chiometric molar ratios of high-purity precursor salts of Y(NO3)3 4H2O (ALDRICH, 99.9%), Al(NO3)3 9H2O (ALDRICH, 99.9%), Tm(NO3)3 5H2O (ALDRICH, 99.9%) and Yb(NO_3)$_3$ 5H_2O (ALDRICH, 99.9%) materials were mixed and dissolved in 25 ml of 1 M HNO3 and then stirred for three hours at a temperature of 353 K. Citric acid, with a molar ratio of metal ions to citric acid of 1:2, was later added to the solution, which was stirred and heated at 363 K until reaching the transparency of the solution. Afterwards, 4 mg of polyethylene glycol was added to the solution, helping to create a gel that was annealed at 673 K for six hours in order to remove the residual nitrates and organic compounds. The resulting powder sample was finally annealed out at 1473 K for twenty hours. Then, the sample was given a second thermal treatment at 1823 K for twelve hours. The outcome obtained is chemically stable.

Powder X-ray diffraction data were collected on a PANalytical X'Pert PRO diffractometer (Bragg-Brentano geometry) with an X'Celerator detector employing the Cu K 1 radiation (= 1.5405) in the angular range 5 < 2 < 80 , by continuous scanning with a step size of 0.02 , achieving the orthorhombic phase in the sample as well as the crystallite size around 40 nm reported in previous works working with the same host material with others lanthanide ions [11,18]. In addition, TEM image of the same host matrix undoped and doped with another lanthanide ion was reported, showing the morphology of such nanomaterial [19].

3.2. Optical measurements

The luminescence measurements were performed from room temperature (RT) up to 470 K in a tubular furnace, where a thermocouple was placed to read the exact temperature of the sample. The excitation of the sample was carried out with a 975 nm diode laser, which was collimated by a lens (f = 75mm) and then focused with a second lens (f = 200 mm) placed so that its back focal point is just in the centre of the furnace, where the sample was located. It should be noticed that the power density at which the temperature calibration was made about 8.0 W/cm^2 in order to avoid the heating of the sample. The luminescence from the sample was focalized at the tip of an optical fiber located in the opposite side of the furnace with a 60 mm focal length lens. Before being focused, the emission was collimated with a lens (f = 200 mm), and then filtered with an 800 nm short pass filter. The optical fiber was coupled to a single grating CCD spectrometer (Andor SR-3031-B CCD Newton DU920N). The heating of the sample was performed at a rate of 0.83 K/min, from RT to 470 K, and the detection was carried out with a resolution of 0.7 nm and an integration time of 10 s. This experiment allowed to calibrate the optical sensor with temperature.

Once the optical sensor was calibrated with temperature, it was possible to monitor the temperature of the nanoperovskite from RT to 430 K by heating the sample with the laser excitation source. The excitation intensity at 975 nm was varied changing the pump power of the laser. The Gaussian beam was focused in the sample with a 75 mm lens and the waist spot size on the sample (defined as the $1/e^2$ radius of the intensity) was 50 50 m^2. Then, the emission was focused on the tip of an optical fiber with a 50 mm focal length lens, previously filtered by an 800 nm short pass filter and recorded by the same spectrometer used in the calibration procedure of the optical sensor.

4. Results and discussion

4.1. Upconversion emission

The emission spectrum of the YAP:Yb-Tm nanocrystal at room temperature excited at 975 nm is shown in Fig. 3. The emission bands centered at 475, 650, 700 and 800 nm are assigned to the $^1G_4$ $^3H_6$, $^1G_4$ $^3F_4$, $^3F_{2,3}$ $^3H_6$ and $^3H_4$ $^3H_6$ transitions, respectively. As it is known, in systems codoped with Yb^{3+}-Tm^{3+}, the $^1G_4$ level of the thulium is populated by an upconversion process of three photons, and the $^3H_4$ level is populated by an upconversion process of two photons [20]. This upconversion mechanism is depicted in Fig. 1. The Yb^{3+} ions absorb laser photons as they have a great absorption cross section at 975 nm. Therefore, one excited Yb^{3+} ion excites the ground state of the Tm^{3+} to the $^3H_5$ state. Then, due to its proximity, the $^3F_4$ state of the Tm^{3+} ions is populated by multiphonon relaxation processes. A second energy transfer process from another excited Yb^{3+} ion populates the $^3F_{2,3}$ state of Tm^{3+} ions, which generates the 700 nm emission band. Moreover, non-radiative relaxation from $^3F_{2,3}$ cause the population of the $^3H_4$ state of Tm^{3+} ions, resulting in the 800 nm emission band [21]. Finally, a third transfer from Yb^{3+} to the $^3H_4$ state populates the $^1G_4$ level.

The inset of Fig. 3, shows the dependence of the upconversion (UC) emission intensities with the excitation power, being n the number of absorbed photons per UC emitted photon. As it has been explained, n values close to 2 and 3 are expected for the 800 and 475 nm emission bands respectively, but as can be seen in Fig. 3 lower values were obtained [22]. This fact could be related to saturation effects of the Yb^{3+} and the first excited state of Tm^{3+} [23].

The emission bands at 700 nm ($^3F_{2;3}$ $^3H_6$) and 800 nm ($^3H_4$ $^3H_6$) are proved to be appropriate for optical temperature sensing, because $^3F_{2,3}$ and $^3H_4$ energy levels are thermally coupled [24]. Fig. 4 shows the 700 and 800 nm emission bands for two different temperatures. It can be seen that the intensity of the 700 nm emission band increases with temperature, while the 800 nm emission band remains quite constant with temperature. This fact is due to the thermally population described before.

4.2. Calibration methods

In this section, two different calibration procedures based in the FIR technique were considered. The first one consists on the determination

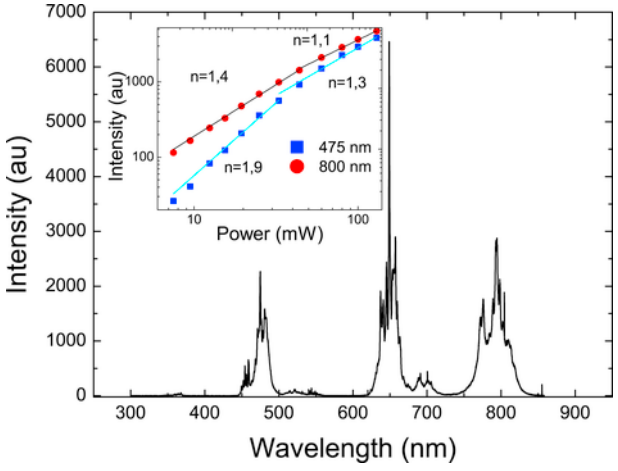

Fig. 3. Room-temperature upconversion emission spectrum of the YAP:Yb-Tm nanocrystals obtained under a pump power of 80 mW at 975 nm. The inset shows the dependence of the upconversion emission with the excitation power in a logarithmic scale.

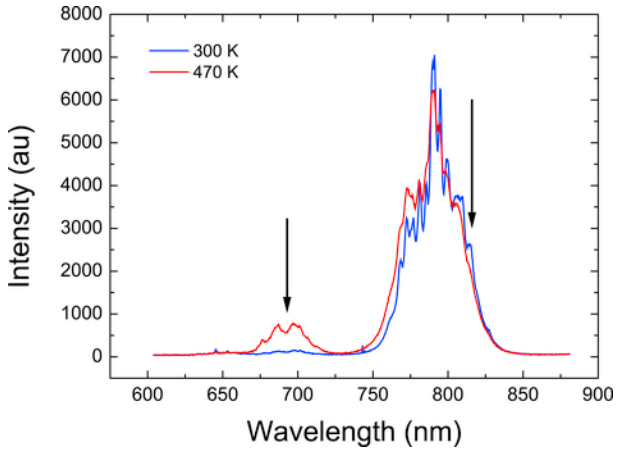

Fig. 4. Luminescence spectra for two different temperatures under 975 nm diode laser excitation. The arrows show the peaks used in the second method of the FIR technique: 690 and 815 nm respectively.

of the emission intensities by the integration of each band. The ratio of these bands (R_1) is described by the Boltzmann distribution according to Eq. (1) and it is shown in Fig. 5. Fitting the experimental ratios to an exponential function, the values C = 1.94 and E = 1173 cm^{-1} have been obtained. The relative sensitivity S_{R1} was calculated according to Eq. (5), being 0.019 K^{-1} the maximum value of this magnitude at 293 K (see Fig. 5). S_{R1} is related to intensity ratios modelled by Eq. (1) and is given by E/KT^2. The YAP produce a high splitting among the $^3F_{2,3}$ and $^3H_4$ levels and consequently a high value for the relative thermal sensitivity.

Other works have explored the possibility to predict the calibration curve in this first calibration using other methods [25]. Assuming that for a low enough excitation pump power there is no laser heating effect and the temperature of the sample is T_0. Then when the sample is heated the temperature can be obtained using Eq. (1) by Ref. [25]:

$$\frac{1}{T} = \frac{1}{T_0} + \frac{K_B}{\Delta E} ln\left(\frac{R}{R_0}\right) \quad (7)$$

As it can be seen, it is not necessary to know the value of the constant C to determine the absolute temperature. However, the value of E needs to be calculated, as example, using the absorption spectra. This energy gap between the thermalized energy levels can be estimated from the spectral positions of the centroids of the absorption bands corresponding to the transitions between the thermalized energy levels. In this way a value of 1776 cm^{-1} has been obtained and it is not

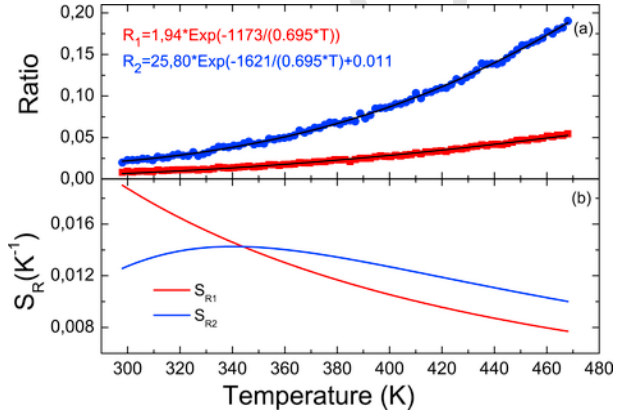

Fig. 5. Fluorescence intensity ratios (a) and relative sensitivities (b) for the two calibration methods as function of the temperature in the range of 300 470 K.

in very good agreement with the value of 1173 cm^{-1} (obtained from fitting procedure). This discrepancy can be explained in basis to the Stark sub-levels that are observed in each band. In other previous works have been also different concordances among the E values obtained from the absorption bands or from the fitting procedure (see Table 2 in Ref. [26]).

Concerning the second calibration procedure, the ratio of two spectra recorded at low and high temperatures was obtained and it is shown in Fig. 6. It can be seen that the maximum and minimum rates were found at about 690 and 815 nm, and so these wavelengths were selected to study their intensity ratio versus temperature. The ratio (R_2) calculated by this method can be described according to the Boltzmann s law plus a constant (D) as it is shown in Fig. 5. The use of an additional constant in Eq. (1) for this second method is justified considering that at 690 nm, there is a little contribution of the emission centered at 650 nm. Therefore, in order to improve this effect, the constant D was added (see Ref. [17]). From this calibration procedure, the values C = 25.80 and E = 1621 cm^{-1} and the additional constant D = 0.0112 have been obtained. The relative sensitivity S_{R2} reaches a maximum value of 0.014 K^{-1} at 340 K (see Fig. 5). According to Fig. 5, the first calibration procedure is better in the range between RT up to 340 K, while the second one is better in the range between 340 and 470 K. In Table 1, a comparison of the values of the relative sensitivity obtained for other nanocrystals doped with rare earth ions is presented. From this table and the relative sensitivities shown in Fig. 5b, it can be concluded that YAP:Yb-Tm reaches a maximum value of the relative sensitivity in the physiological range which is higher than the values obtained in other rare earth doped nanocrystals. As can be seen in Fig. 5b, a combination of the two calibration methods R_1 and R_2 leads to a relative sensitivity larger than $10^{-2} K^{-1}$ in the range between 340 and 470 K.

The intensity ratios and temperature uncertainties were estimated for both calibration methods by using the procedure described in Ref. [17]. The intensity ratio uncertainties range from 1% (T = 300 K) to 4% (T = 470 K) for the calibration 1 and from 2.6% (T = 300 K) to 0.6% (T = 470) for the calibration 2. Respect to temperature uncertainties, we have evaluated Eq. (6) obtaining values ranging from 0.5 K (T = 300 K) to 5 K (T = 470 K) for the calibration 1. On the other hand, for the calibration 2 the uncertainties vary from 2 K (T = 300 K) to 0.7 K (T = 470 K). We can conclude that if we combine both combination procedures the temperature uncertainty can be kept below 1 K in all the temperature range (300 470 K).

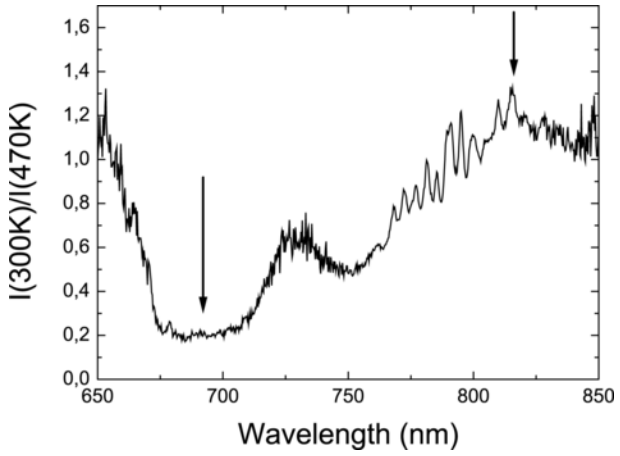

Fig. 6. Ratio of upconversion spectra obtained at two different temperatures (300 and 470 K). The wavelengths used for the second calibration method R_2 are marked with arrows.

Table 1
Maximum relative sensitivity for different RE^{3+} temperature optical sensors in the physiological range

Optical sensor	range (nm)		Temp.	Exc	Maximum *SREL* within the physiological range	Ref.
	Upper energy level	Lower energy level	range (K)	(nm)	(303 318K) (x$10^{-3}K^{-1}$	
YAP:Yb-Tm (nano)	675 725	750 825	298 470	975	18 (R1)	This work
	690	815	298 470	975	14 (R2)	
YAP:Tm (nano)	792 800	800 803	294 324	1210	10	[8]
Na2Y2B2O7: Er^{3+}/Yb^{3+} nanophosphor	510 536	538 572	300 613	980	8.3	[27]
CaMoO4: Er^{3+}/Yb^{3+} nanophosphor	517 542	543 578	300 535	980	5.9	[28]
CaF2: Tm/Yb (nano)	785 795	795 805	299 323	920	2.4	[29]
LiNdP4O12 (nano)	880 890	890 920	250 500	808	2.3	[30]
NaYF4: Nd (nano)	860 864	865 880	273 423	830	1.3	[31]
YAG: Nd (nano)	935 941	943 950	283 343	808	1.2	[32]
LaF3: Nd (nano)	855 874	875 890	283 333	808	1	[33]

It can be seen in Fig. 5a, that small oscillations appear in R_2 as compared with R_1. These small oscillations can be produced by peaks shifts or splitting of energy sublevels that change with the temperature. Nevertheless, the values of these oscillations are in the range of the uncertainties previously estimated.

4.3. Laser heating

The previous calibration processes have been made by exciting the sample with a low pump power in order to do not heat the sample. It must be taken into account that nonradiative processes that involve emission phonons can produce heating of the matrix. In some experiments, however, it is interesting to control the temperature of the sample by changing the excitation pump power. Therefore, the upconversion emission spectra for excitation at 975 nm and different powers were recorded and the temperature of the sample was estimated using the calibration method R_2. Considering the experimental conditions detailed in the experimental section, the sample absorbed around 50% of the 186 mW excitation power, achieving a temperature around 430 K. In Fig. 7 both the measurements of the ratio of intensities for different values of the laser power and the inferred temperature values are presented in the heating and cooling processes. It can be seen that a good agreement in the values has been obtained for both procedures. Thus, with this technique the sample temperature can be properly monitored in the range from 300 to 430 K.

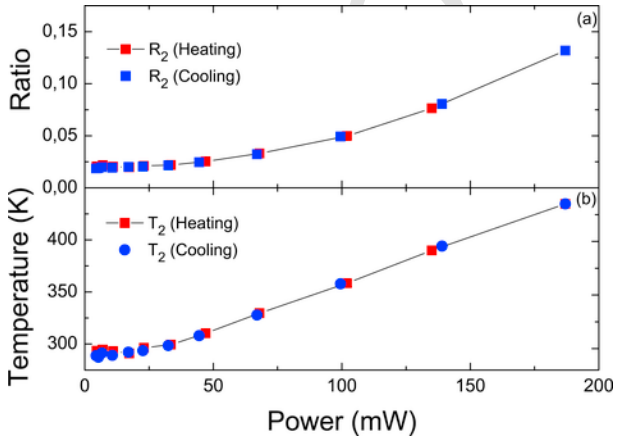

Fig. 7. Intensities ratios (a) and temperature induced (b) obtained by R_2 calibration on the sample by the laser heating as a function of the pump power. Both heating and cooling processes are shown.

5. Conclusions

The thermal sensing capability of the YAP:Yb-Tm was studied in order to check its viability as an optical temperature sensor. Two different calibration procedures based in the FIR technique were carried out, resulting in two different relative sensitivities: S_{R1} reaches a maximum value of 0.019 K^{-1} at the lowest temperature, while S_{R2} reaches a maximum value of 0.014 K^{-1} at 340 K. The conventional FIR technique (R_1) has its better sensitivity in the range from RT to 340 K, and the second method here proposed (R_2) performs better from 340 to 470 K. If a combination of both methods is used, the relative sensitivity will stay above 10^{-2} K in the whole temperature range. In addition, the laser induced heating effect in YAP:Yb-Tm has been studied, and the temperature of the sample has been estimated in the heating and cooling process, obtaining a good agreement between them. These features confirm the potential utility of YAP:Yb-Tm as an optical thermal sensor for biological applications.

Acknowledgments

This research was partially supported by Ministry of Education and Science of Russia (grant 14.Z50.31.0009), by the Spanish MINECO (MAT2015-71070-REDC, and MAT2016-75586-C4-4-P, FIS2016-77319-C2-1-R), and by the EU-FEDER funds.

References

[1] G. Adam, J. Gibbs, J. Chem. Phys. 43 (1965) 139.
[2] H. P rtner, Comp. Biochem. Physiol. Mol. Integr. Physiol. 132 (2002) 739.
[3] B. Rubinsky, G. Onik, Int. J. Refrig. 14 (1991) 190.
[4] D. Needham, M. Dewhirst, Adv. Drug Deliv. Rev. 53 (2001) 285.
[5] Y. Zhou, F. Qin, Y. Zheng, Z. Zhang, W. Cao, Opt. Lett. 40 (2015) 4544.
[6] S. Zhou, X. Li, X. Wei, C. Duan, M. Yin, Sensor. Actuator. B Chem. 231 (2016) 641.
[7] V. Rai, S. Rai, Spectrochim. Acta. A. Mol. Biomol. Spectrosc 68 (2007) 1406.
[8] M. Hern ndez-Rodriguez, A. Lozano-Gorr n, V. Lav n, U. Rodr guez-Mendoza, I. Mart n, Optic Express 25 (2017) 27845.
[9] L. Xing, Y. Xu, R. Wang, W. Xu, Z. Zhang, Opt. Lett. 39 (2014) 454.
[10] A. Pereira, K. Kumar, W. Silva, W. Santos, D. Jaque, C. Jacinto, Sensor. Actuator. B Chem. 213 (2015) 65.
[11] M.A. Hern ndez-Rodr guez, V. Monteseguro, A.D. Lozano-Gorr n, F.J. Manj n, J. Gonz lez-Platas, P. Rodr guez-Hern ndez, A. Mu z, V. Lav n, U.R. Rodr guez-Mendoza, J. Phys. Chem. C 121 (2017) 15353.
[12] M.S. Marques, L.D.S. Menezes, W. Lozano B, L.R.P. Kassab, C.B. De Ara jo, J. Appl. Phys. 113 (2013) 053102.
[13] R. Moncorg , B. Chambon, J.Y. Rivoire, N. Garnier, E. Descroix, P. Laporte, H. Guillet, S. Roy, J. Mareschal, D. Pelenc, J. Doury, P. Farge, Opt. Mater. 8 (1997) 109.
[14] M. Weber, M. Bass, K. Andringa, R. Monchamp, E. Comperchio, Appl. Phys. Lett. 15 (1969) 342.

[15] V. Rai, Appl. Phys. B 88 (2007) 297.
[16] S. Wade, S. Collins, G. Baxter, J. Appl. Phys. 94 (2003) 4743.
[17] C.D.S. Brites, A. Millan, L.D. Carlos, Lanthanides in luminescent thermometry, in: J.V.G. B nzli, V.K. Pecharsky (Eds.), Handbook on the Physics Chemistry of the Rare Earths: Including Actinides, Elsevier B.V., Amsterdam, 2016, pp. 339–427.
[18] M.A. Hern ndez-Rodr guez, A.D. Lozano-Gorr n, I.R. Mart n, U.R. Rodr guez-Mendoza, V. Lav n, J. Lumin. 188 (2017) 204.
[19] M.A. Hern ndez-Rodr guez, A.D. Lozano-Gorr n, I.R. Mart n, U.R. Rodr guez-Mendoza, V. Lav n, Sensor. Actuator. B Chem. 255 (2018) 970.
[20] K. Kumar, W. Silva, K. Venkata Krishnaiah, C. Jayasankar, C. Jacinto, J. Nanophotonics 8 (2014) 083093.
[21] D. Simpson, W. Gibbs, S. Collins, W. Blanc, B. Dussardier, G. Monnom, P. Peterka, G. Baxter, Optic Express 16 (2008) 13781.
[22] M. Pollnau, D. Gamelin, S. L thi, H. G del, M. Hehlen, Phys. Rev. B Condens. Matter 61 (2000) 3337.
[23] C. Jacinto, M. Vermelho, E. Gouveia, M. de Araujo, P. Udo, N. Astrath, M. Baesso, Appl. Phys. Lett. 91 (2007) 071102.
[24] W. Xu, X. Gao, L. Zheng, Z. Zhang, W. Cao, Sens. Actuators, B 173 (2012) 250.
[25] S. Balabhadra, M.L. Debasu, C.D.S. Brites, R.A.S. Ferreira, L.D. Carlos, J. Phys. Chem. C 121 (2017) 13962.
[26] W. Xu, D. Li, H. Hao, Y. Song, Y. Wang, X. Zhang, Opt. Mater. 78 (2018) 8.
[27] A. Soni, V. Rai, M. Mahata, Mater. Res. Bull. 89 (2017) 116.
[28] S. Sinha, M. Mahata, K. Kumar, S. Tiwari, V. Rai, Spectrochim. Acta. A. Mol. Biomol. Spectrosc 173 (2016) 369.
[29] N. Dong, M. Pedroni, F. Piccinelli, G. Conti, A. Sbarbati, J. Ram rez-Hern ndez, L. Maestro, M. Iglesias-de la Cruz, F. Sanz-Rodriguez, A. Juarranz, F. Chen, F. Vetrone, J. Capobianco, J. Sol , M. Bettinelli, D. Jaque, A. Speghini, ACS Nano 5 (2011) 8665.
[30] L. Marciniak, K. Prorok, A. Bednarkiewicz, A. Kowalczyk, D. Hreniak, W. Strek, J. Lumin. 176 (2016) 144.
[31] D. Wawrzynczyk, A. Bednarkiewicz, M. Nyk, W. Strek, M. Samoc, Nanoscale 4 (2012) 6959.
[32] A. Benayas, B. del Rosal, A. P rez-Delgado, K. Santacruz-G mez, D. Jaque, G. Hirata, F. Vetrone, Adv. Opt. Mater 3 (2015) 687.
[33] U. Rocha, C. Jacinto Da Silva, W. Ferreira Silva, I. Guedes, A. Benayas, L. Mart nez Maestro, M. Acosta Elias, E. Bovero, F.C.J.M. Van Veggel, J.A. Garc a Sol , D. Jaque, ACS Nano 7 (2013) 1188.